PERGAMON

International Journal of Solids and Structures 36 (1999) 1169–1191

INTERNATIONAL JOURNAL OF SOLIDS and STRUCTURES

Combination of fracture and damage mechanics for numerical failure analysis

J. C. W. van Vroonhoven[a,*], R. de Borst[b]

[a]*Philips Research Laboratories, Prof. Holstlaan 4, 5656 AA Eindhoven, The Netherlands*
[b]*Eindhoven University of Technology, Faculty of Mechanical Engineering, P.O. Box 513, 5600 MB Eindhoven, The Netherlands and Delft University of Technology, Faculty of Civil Engineering, P.O. Box 5048, 2600 GA Delft, The Netherlands*

Received 21 May 1997; in revised form 29 October 1997

Abstract

A new approach for the analysis of crack propagation in brittle materials is proposed, which is based on a combination of fracture mechanics and continuum damage mechanics within the context of the finite element method. The approach combines the accuracy of singular crack-tip elements from fracture mechanics theories with the flexibility of crack representation by softening zones in damage mechanics formulations. A super element is constructed in which the typical elements are joined together. The crack propagation is decided on either of two fracture criteria; one criterion is based on the energy release rate or the *J*-integral, the other on the largest principal stress in the crack-tip region. Contrary to many damage mechanics methods, the combined fracture/damage approach is not sensitive to variations in the finite element division. Applications to situations of mixed-mode crack propagation in both two- and three-dimensional problems reveal that the calculated crack paths are independent of the element size and the element orientation and are accurate within one element from the theoretical (curvilinear) crack paths.

1. Introduction

Various numerical approaches have been developed for the analysis of crack propagation in complex mechanical structures consisting of brittle, linearly elastic materials. These approaches can be divided into two categories: those based on fracture mechanics and those based on continuum damage mechanics. In this paper we shall briefly discuss both theories, fracture and damage, and their particular advantages and disadvantages in finite element applications. The purpose of the present paper is to describe a numerical tool for the analysis of (dynamic) crack

*Corresponding author.

0020–7683/99/$ - see front matter
PII: S0020–7683(97)00345–4

propagation, based on the finite element method and on a combination of fracture mechanics principles and damage mechanics principles. This combination will be chosen such that the disadvantages of fracture and damage mechanics in a finite element method are eliminated, while their specific benefits are retained.

The major advantage of fracture mechanics approaches is that they have been studied extensively such that a broad range of applicability has been found. These approaches are based on the finite element method which is commonly used for the solution of complicated mechanical problems including non-linear constitutive behaviour and/or large geometries (Hughes, 1987; MacNeal, 1994). In order that the numerical solution incorporates the stress singularity which arises at the crack tip in linear elasticity theory, Barsoum (1976), Stern and Becker (1978), and Stern (1979) have developed special finite elements which are positioned at the crack tip, and which possess a high degree of accuracy. A strong disadvantage occurs when such numerical methods are applied to problems of dynamic fracture. Because of the material rupture and the creation of new crack surfaces, the geometry of the elastic body changes continuously. As a result, the finite element division requires continuous adaptation, including a translation of the special crack-tip elements with the moving crack tip. Such moving finite element techniques often assume that the crack path is straight or otherwise known beforehand (Nishioka et al., 1990). Since crack propagation along arbitrary curved paths requires the adaptation of many finite elements, the use of fracture mechanics approaches is generally restricted by the large computational efforts involved in the adaptations of the element divisions. In order to avoid these difficulties, van Vroonhoven (1996a, b) and van Vroonhoven and de Borst (1997) proposed an uncoupled numerical fracture method, in which the dynamic effects (such as wave propagation) and the crack propagation have been partially uncoupled. This method produces reliable results for the initial stages of crack propagation, but due to the uncoupling of the dynamic effects, deviations in the crack paths occur near the moment of crack arrest or final collapse. In order to include the interaction between the dynamic effects and the crack propagation in a coupled approach, the possible application of continuum damage mechanics is investigated.

Approaches based on continuum damage mechanics have an advantage over those based on fracture mechanics, in the sense that continuous adaptation of the finite element division has become superfluous because material failure is represented by internal damage and changes in the geometry do not occur. There also exist some complications, however. In particular, severe material degradation may lead to softening behaviour: the internal stresses decrease with increasing strain. As a result, the mathematical formulation of the boundary value problem becomes ill-posed. In such cases it is often seen that the damage increase is highly susceptible to small variations in the local stress values and in the finite element division, leading to pathological element dependencies. On one hand, these dependencies concern the width of the damaged zone: refinement of the element division generally leads to higher values of the damage in a region of smaller width. This effect is referred to as "localization" and has been studied by various authors, among others by Bažant and Cedolin (1991), de Borst (1993), de Borst et al. (1993), Lasry and Belytschko (1988), Mühlhaus (1989), Needleman (1988), and Sluys (1992). On the other hand, the orientation of the finite elements plays an important role: it is often seen that damage progresses along element boundaries and not in the required direction as derived from a fracture mechanics analysis. These problems even occur for simple geometries and restrict the applicability of continuum damage mechanics in its original form.

In order to make profitable use of the positive aspects of both theories, the idea of a combined fracture/damage approach for the analysis of failure phenomena has been proposed by Horsten and van Vroonhoven (1994), van Vroonhoven (1996a), and van Vroonhoven and Horsten (1996). The numerical approach proposed in this paper is based on their idea and consists of the following steps. Subsequent positions of the crack tip are calculated using fracture mechanics and special finite elements, such that the crack path is known at every moment of the fracture process and with highest possible accuracy. Large-scale adaptations of the finite element division are avoided by the use of continuum damage mechanics to describe the "tail" of the crack. At these positions the Young's modulus of elasticity is reduced in the direction perpendicular to the crack surfaces. In fact, one should not speak of a crack in the strict sense but of a damaged zone, since there is no geometrical discontinuity in the material. This combined approach unites the accuracy of the special crack-tip elements in fracture mechanics with the flexibility of crack representation in damage mechanics and is an effective means for the analysis of crack propagation by the finite element method. We shall investigate the possible dependencies on the element division, which often occur in damage mechanics applications. Such dependencies should not be present to ensure the correctness of the combined fracture/damage approach.

2. Discussion of fracture and damage mechanics

Fracture mechanics methods are characterized by the assumption of a sharp crack in an elastic body. The deformation of the elastic body is expressed in terms of displacements u_i, strains ε_{ij}, and stresses σ_{ij} with indices $i, j = 1, 2, 3$ or x, y, z. The crack introduces a material discontinuity and, within the scope of linear elasticity theory, the crack tip becomes a singular point where the stresses attain infinite values. The singular behaviour of the stress components is proportional to the inverse square root of the distance r to the crack tip and the singularity is normalized by stress intensity factors. When the crack surfaces are positioned along the negative x-axis with the crack front along the z-axis and with the crack tip at the origin, the singular stress behaviour can be represented in the simplified form

$$\sigma_{ij}(r,\theta) = \frac{K}{\sqrt{2\pi r}} f_{ij}(\theta), \tag{1}$$

where K is a stress intensity factor related to the external forces and the boundary conditions. Three stress intensity factors exist: K_{I}, K_{II}, and K_{III}, each associated with a different fracture mode. The angular variations $f_{ij}(\theta)$ are well-known functions of the polar angle θ, depending on the fracture mode, and are given by Broek (1986) and Cherepanov (1979).

The stress singularity introduces two complications. Firstly, the yield stress will be exceeded at positions sufficiently close to the crack tip. Fortunately, England (1965) and Rice (1968) have shown that fracture of brittle materials involves only limited plasticity or small-scale yielding confined to a very small neighbourhood of the crack tip. Secondly, standard finite elements have linear or quadratic interpolation of the displacements and, consequently, constant or linear internal stresses. These elements are thus inappropriate for an accurate description of the near-tip variables and special finite elements have been developed. For example, Stern and Becker (1978) and Stern (1979) have suggested the use of square-root functions $\sqrt{r}$ for the interpolation of the displacements

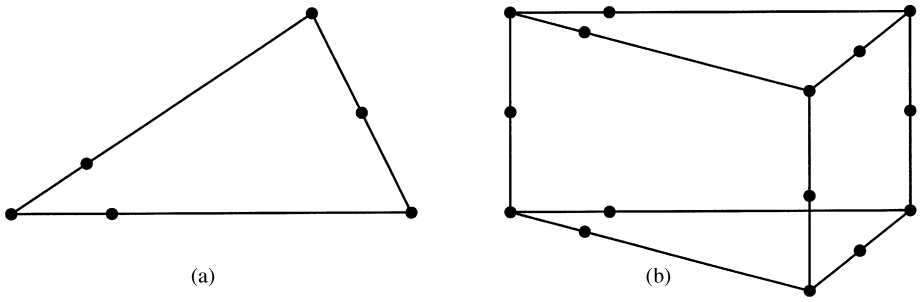

Fig. 1. Collapsed elements in (a) two and (b) three dimensions.

in triangular five-node and six-node elements. Barsoum (1976) has suggested the use of collapsed quadrilateral eight-node elements with quarter-point nodes on the element sides adjacent to the crack tip. The resulting element has a triangular shape and is shown in Fig. 1. In three-dimensional fracture problems, collapsed hexahedral 20-node elements are used. The onset of fracture and the direction of crack propagation are usually determined from the magnitude and the ratio of the stress intensity factors (Broek, 1986; Cherepanov, 1979) or from a criterion based on energetic principles (Cherepanov, 1979; Freund, 1990; Rice, 1968).

Damage mechanics methods are characterized by the assumption of a smeared crack where the material remains continuous, while the material strength decreases due to internal damage. A parameter D is introduced to represent the material degradation; see for example Chaboche (1981, 1988a, b), Kachanov (1958) and Lemaitre (1984). Material damage that occurs in some anisotropic fashion can be represented by a set of damage parameters, such as a vector D_i or a tensor D_{ij} (Chaboche, 1981; Murakami, 1988). The softening behaviour of a deformable body subjected to uniaxial loading is governed by the following constitutive relation between the stress σ and the strain ε in a simple one-dimensional form:

$$\sigma = (1-D)E\varepsilon, \tag{2}$$

where E is the Young's modulus pertaining to the original, undamaged material. This relation is illustrated in Fig. 2 for general ductile failure and for brittle failure. Generally, the damage parameter D at time t depends on the history of the strain. According to Chaboche (1998b), the maximum strain level in time serves as a threshold for the damage increase for a certain class of materials and we may write $D(t) = D(\varepsilon_{\max})$ with $\varepsilon_{\max}(t) = \max\{\varepsilon(t_1)|t_1 \leqslant t\}$. The relation between

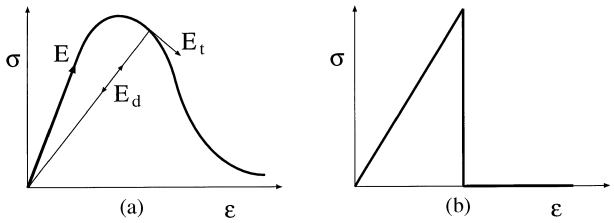

Fig. 2. Stress–strain relations with softening material behaviour for (a) ductile and (b) brittle failure.

D and $\varepsilon_{\max}$ is usually postulated on the basis of experimental results. For situations where both the strain and the damage increase monotonically, we may write $D = D(\varepsilon)$ because $\varepsilon_{\max}(t) = \varepsilon(t)$.

We distinguish several moduli, depending on the loading situation. Firstly, when the body is loaded or unloaded and damage does not occur ($D = 0$), we use the original Young's modulus E and we have the stress–strain relation $\sigma = E\varepsilon$. Secondly, when the body is loaded and the damage increases ($\dot{\varepsilon} > 0$ and $\dot{D} > 0$), the stress–strain relation is written in incremental form: $\dot{\sigma} = E_t \dot{\varepsilon}$, and we use the tangent modulus

$$E_t = \frac{\mathrm{d}\sigma}{\mathrm{d}\varepsilon} = ((1-D) - D'(\varepsilon)\varepsilon)E, \tag{3}$$

where the prime $'$ indicates differentiation with respect to ε. Thirdly, when damage has occurred and the body is unloaded ($\dot{\varepsilon} < 0$), we use the effective modulus $E_d = (1-D)E$ of the damaged material. The stress–strain relation in this case is given by $\sigma = E_d\varepsilon$ and is also valid for reloading as long as damage increase does not occur, i.e., as long as $\varepsilon(t) < \varepsilon_{\max}(t)$.

It is evident from (3) that the tangent modulus may become negative when the damage D and the damage increase $D'(\varepsilon)$ are too large. A negative tangent modulus has the severe implication that one-dimensional dilatational wave speed c_d, which is defined by

$$c_d^2 = \frac{E_t}{\rho}, \tag{4}$$

becomes imaginary. The corresponding wave equation changes its type from hyperbolic to elliptic and the mathematical problem becomes ill-posed, which leads to several peculiar "localization" phenomena. For example, the energy dissipation associated with the damage increase takes place in an infinitesimally small band (which can be compared to a discrete crack) and the strain in this band attains an infinite value, while the strain in the surrounding material decreases (unloading). As a consequence, in finite element applications, a strong dependence on the size of the softening elements is observed regarding the amount of dissipated energy, the global structural response, and the peak value of the strain after localization. An overview of localization problems is given in the work of Bažant and Cedolin (1991). Various solutions have been suggested, which include:

(1) rate-dependent models where the stresses not only depend on the strains but also on the strain rate (Sluys, 1992; Needleman, 1988);
(2) gradient-dependent models where the stresses depend on the strains and on the spatial derivatives of the strains (de Borst et al., 1993; Lasry and Belytschko, 1988; Sluys, 1992);
(3) Cosserat models where couple-stresses and microcurvatures are added to represent the underlying microstructure (Mühlhaus, 1989; de Borst, 1993).

3. Description of the combined approach

From the preceding discussion it is clear that both fracture mechanics and continuum damage mechanic possess specific advantages and disadvantages in finite element applications. Whereas numerical methods based on fracture mechanics require frequent adaptations of the finite element division and use moving element techniques (Nishioka et al., 1990), methods based on damage

mechanics suffer from sensitivity with respect to the element division and from damage localization. Because of these complications, a combination of fracture and damage mechanics within the context of the finite element method is investigated. The combined fracture/damage approach is based on the finite element method plus a time-step algorithm and combines the accuracy of fracture mechanics with the flexibility of continuum damage mechanics. For the sake of simplicity, we start with two-dimensional (plane stress) problems.

3.1. *Construction of super element*

As in any finite element analysis, we start with the division of the elastic body into subdomains. We choose the improved four-node elements developed by Wilson et al. (1973) and Taylor et al. (1976); see also MacNeal (1994). These elements have an improved bending stiffness so that the displacements and the stresses are calculated correctly in the case of bending deformation. The performance of these so-called Wilson–Taylor elements in such cases is far better than the performance of standard four-node linear elements and is comparable to the performance of eight-node quadratic elements (van Vroonhoven, 1996a). The singular elements for fracture mechanics applications (Barsoum, 1976; Stern and Becker, 1978; Stern, 1979) are used at the crack tip by replacing the original quadrangular element with four collapsed, triangular elements. One crack-tip node, twelve mid-side nodes, and four quarter-point nodes are added to ensure the accurate calculation of the singular stresses in the vicinity of the crack tip. The additional nodes are marked by open circles (○) in Fig. 3 and the original nodes by filled dots (●). Since the displacements in the singular elements are interpolated by quadratic shape functions on the sides opposite to the crack tip, it is necessary to apply variable-node elements (Hughes, 1987) as a transition from the singular elements to the four-node elements. This combination of the four crack-tip elements and the eight surrounding transitional elements is called a "super element". The transitional variable-node elements and the singular crack-tip element have 3×3 Gaussian integration points, while the Wilson–Taylor elements have 2×2 Gaussian integration points. The positions of the four corner nodes of the quadrangular element which is replaced with the singular elements, are adjusted in such a manner that the four triangular elements have approximately the same size. The super element translates with the crack tip and its structure is similar to the element patterns which are used in moving finite element procedures based on fracture mechanics.

The additional nodes are regarded as "slave" nodes, as opposed to the original "master" nodes of the elements. The slave nodes are eliminated at the super element level by means of static condensation (Hughes, 1987). It is noted that the (four) corner nodes of the singular crack-tip elements are also eliminated and must also be regarded as slave nodes. We proceed with the calculation of the internal force vector $\mathbf{H}_m$ associated with the displacements $\mathbf{u}_m$ of the twelve master nodes of the super element. Since the twenty-one slave nodes lie in the interior of the super element, they do not convey nodal forces to the surrounding elements. Denoting the displacements of the slave nodes by $\mathbf{u}_s$, we obtain the following system of equations

$$\begin{bmatrix} K_{mm} & K_{ms} \\ K_{sm} & K_{ss} \end{bmatrix} \cdot \begin{bmatrix} \mathbf{u}_m \\ \mathbf{u}_s \end{bmatrix} = \begin{bmatrix} \mathbf{H}_m \\ \mathbf{0} \end{bmatrix}, \tag{5}$$

where the contributions of the twelve elements in the super element to the stiffness matrix K have

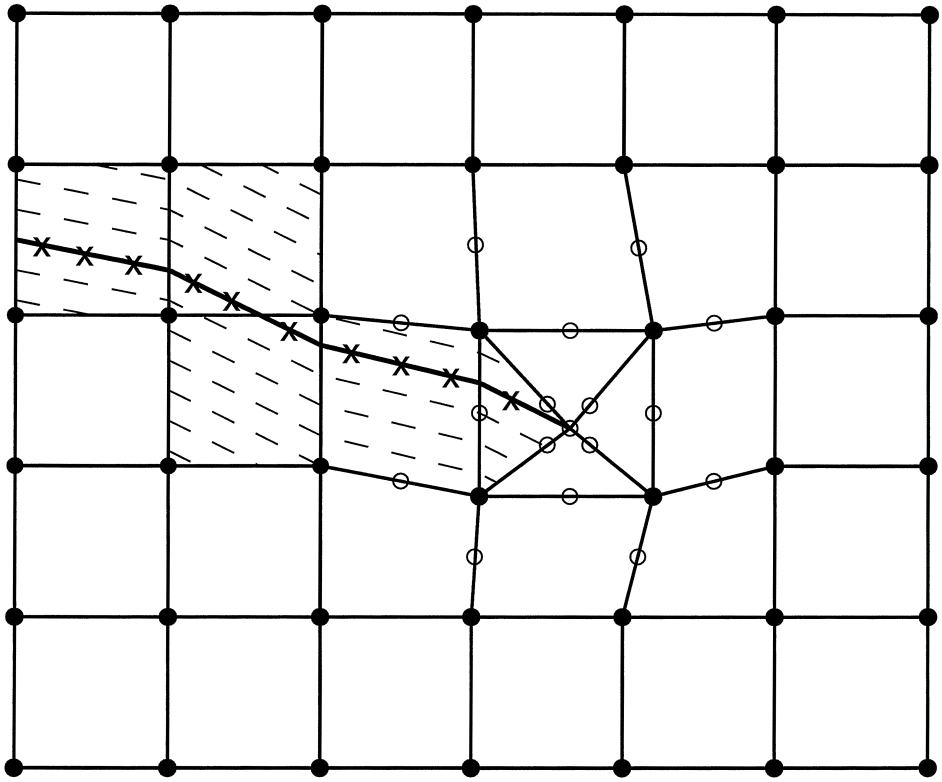

Fig. 3. Configuration of the super element (four crack-tip elements and eight transitional elements) with surrounding elements. The crack is shown as a thick solid line and anisotropic damage is displayed by dashed lines. Subsequent positions of the crack tip are marked as $\times$, while original nodes are indicated by ● and extra nodes by ○.

been partitioned with respect to the master and the slave nodes. Solving the second part of (5) for $\mathbf{u}_s$ and substituting the result into the first part, we obtain an expression for the "condensed" stiffness matrix K^{se} of the super element:

$$\mathbf{H}_m = K^{se} \cdot \mathbf{u}_m = (K_{mm} - K_{ms} K_{ss}^{-1} K_{sm}) \cdot \mathbf{u}_m. \tag{6}$$

A smaller type of super element has also been considered (Horsten and van Vroonhoven, 1994). This super element has two basic configurations; see Fig. 4. When the crack tip is in the middle of an element, that element is split into four triangular crack-tip elements. When the crack tip is near a corner, four elements are split into eight triangles. Quarter-point nodes are added to incorporate the singular stress behaviour, but the extra mid-side nodes are not included. As a result, in either configuration, the triangular elements resemble the element of Fig. 1(a) but without the extra mid-side node on the side opposite to the crack tip. Consequently, the displacements on that side show linear behaviour. This smaller super element did not provide sufficient accuracy near the crack tip and has therefore been rejected. On the other hand, super elements of larger size were regarded as too expensive because of the increase in computational effort and in assembly time.

The position of the crack tip is marked by $\times$ in Fig. 3 and is calculated at every time step by

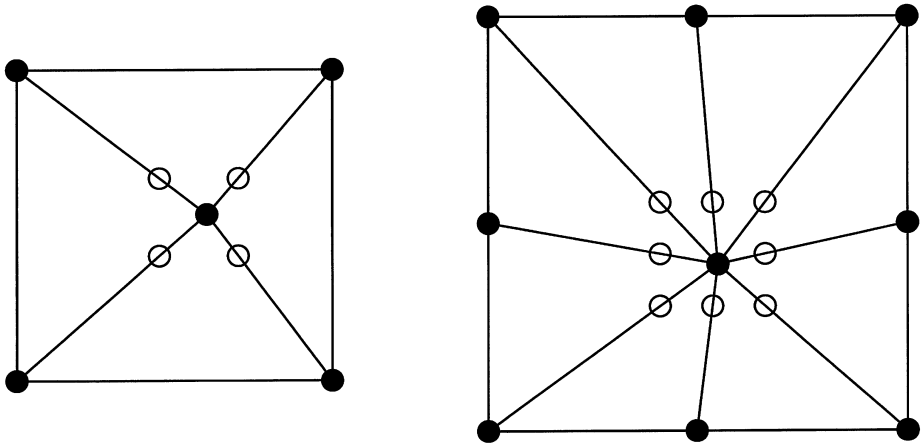

Fig. 4. Configuration of smaller super elements with (a) four and (b) eight crack-tip elements.

the procedure explained below. Although the crack path is determined in a precise manner, it is not approximated by a piece-wise linear curve. Instead, we employ the concept of a "smeared" crack but in a different form than that used by Rots (1991). The smeared crack concept provides extra flexibility in comparison with fracture mechanics procedures which require element splitting or nodal-release techniques. The "tail" of the crack is modelled with the use of damaged elements showing softening behaviour. We assume orthotropic behaviour of the damaged material: the stiffness in the direction perpendicular to the crack is reduced, while the stiffness parallel to the crack retains the original value of the undamaged material. The constitutive equations are given by

$$\begin{bmatrix} \varepsilon_{xx} \\ \varepsilon_{yy} \\ 2\varepsilon_{xy} \end{bmatrix} = \begin{bmatrix} 1/E_x & -\mu_{xy}/E_y & 0 \\ -\nu_{xy}/E_x & 1/E_y & 0 \\ 0 & 0 & 1/G_{xy} \end{bmatrix} \cdot \begin{bmatrix} \sigma_{xx} \\ \sigma_{yy} \\ \sigma_{xy} \end{bmatrix}. \tag{7}$$

The expression for the stress components in terms of the strains is obtained by inversion. The E-moduli represent the tensile stiffness in the coordinate directions, while the G-modulus is related to shear deformation. The parameter ν_{xy} is the contraction ratio in the x-direction when the material is subjected to tension along the y-axis, whereas ν_{yx} is defined reversely. The five elasticity parameters are not independent, because the stress–strain relations (7) must be symmetric. Thus, four independent parameters remain. The presence of a crack implies a local reduction of the stiffness in only one direction. Taking the x-axis in the direction parallel to the crack surfaces, we have for the damaged material that $E_x = E$, $E_y = (1-D)E$, and $\nu_{yx} = \nu$, $\nu_{xy} = (1-D)\nu$, where D is the damage parameter and E and ν are the Young's modulus and the Poisson's ratio of the undamaged material, respectively. The shear modulus G_{xy} is independent of the other parameters and may for example be chosen equal to the arithmetic, geometric, or harmonic mean of the values $E_x/2(1+\nu_{yx})$ and $E_y/2(1+\nu_{xy})$, which are all acceptable choices from a thermodynamics point of

view (van Vroonhoven, 1996a). We take $D = 0.999$ in the numerical calculations, resulting in a reduction of Young's modulus by a factor 1000.

In the construction of the super element it is assumed that a crack is present. At any intermediate time step of the fracture simulation, we take the crack path from the previous time step, which is extended with the calculated crack increment. At the start of the computation we must initiate a crack, whose location, length, and direction may be chosen arbitrarily. There is one restriction: the element containing the crack tip must be surrounded by eight other elements, so that a super element as in Fig. 3 can be created. This restriction also applies during the fracture simulation. When the crack tip approaches the boundary of the elastic body and the construction of a super element is no longer possible, the fracture simulation is terminated. The postulation of an initial crack is a limitation of the combined approach, in the sense that the crack initiation is not determined by continuum damage mechanics methods. This is not regarded as a major limitation, because the location of crack initiation is often known beforehand (e.g. the location of the highest tensile stress) and because fracture mechanics methods instead of damage mechanics methods are used in the crack-tip region to determine the crack propagation. We also emphasize that the present implementation of the combined approach admits the analysis of only one crack at a time. The approach can easily be extended to the analysis of multiple cracks by the creation of multiple super elements.

3.2. *Crack propagation*

We now turn to the selection of a crack propagation criterion. Because of the softening zone, the influence of the crack is smeared out over a band of finite width. The global behaviour of the damaged zone resembles the response of a physical discrete crack. At the more detailed local level, however, there will occur deviations between discrete and smeared cracks. For example, the distributions of the stresses and the strains near the crack path will be less accurate in the case of a smeared crack. As a result, we cannot calculate stress-intensity factors by applying integral expressions to the stresses along the crack, as is usually done in fracture mechanics methods; see for example van Vroonhoven and de Borst (1997). It is the more suitable to employ a criterion which focuses at the crack-tip region where fracture mechanics is applied, such as the fracture criterion based on the energy release rate and the J-integrals (Cherepanov, 1979; Freund, 1990; Rice, 1968). For an infinitesimally small contour C encircling the crack tip and with its end points on the lower and upper crack surfaces, the integrals J_k with index $k = 1, 2$ or x, y are defined by

$$J_k = \int_C ((W+T)n_k - \sigma_{ij} n_j u_{i,k})\, \mathrm{d}s, \tag{8}$$

where n_i denotes the components of the outward normal to the contour and the variables $W = \frac{1}{2}\sigma_{ij}\varepsilon_{ij}$ and $T = \frac{1}{2}\rho \dot{u}_i \dot{u}_i$ are the elastic and kinetic energy densities, respectively, with ρ the density of the elastic material. We employ the Einstein convention of summation over repeated indices and use the notation $,k$ and the superposed dot to indicate differentiation with respect to the coordinate x_k and time t, respectively. The contour for evaluation of the integrals is chosen inside the super element around the crack tip as illustrated in Fig. 5 by a thick solid line; five Gaussian integration points are used for each segment of the contour. The contour passes through

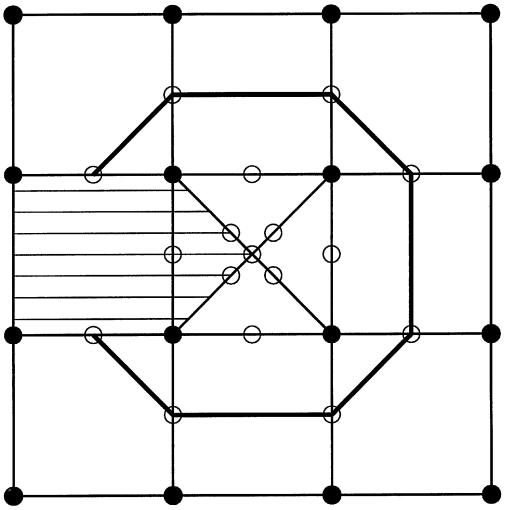

Fig. 5. Contour inside super element for calculation of J-integrals.

the elements which surround the four singular elements, but the contour does not intersect the damaged element. Namely, the integrals J_k must be evaluated for contours around the crack tip from one crack surface to the other and the crack in the combined fracture/damage approach is represented by a damage zone. Thus, the integration is performed from one side of the damaged element through the undamaged material to the other side. Excluding the line segment through the damaged element can also be justified by the following argument. We have the relation (2) in which the damage D increases and the stress σ remains constant due to equilibrium. As a result, there is a large growth of the strain ε in the damaged element and the corresponding line segment would yield an unrealistically large, disturbing contribution to the J-integrals.

The integrals J_k form a vector $\mathbf{J} = J_k \mathbf{e}_k$ with the unit vectors $\mathbf{e}_1$ and $\mathbf{e}_2$ being tangential and perpendicular to the crack path, respectively. Since the integrals have the dimension of energy per unit area, the vector can be interpreted as the energy flux into the crack tip per unit area of newly crated crack surfaces. A well-established criterion for situations of static fracture (Cherepanov, 1979) states that crack extension will occur when the length of the vector $\mathbf{J}$ reaches the critical energy release rate $\mathscr{G}_C$, a material constant, while the crack extends in the direction $\theta = \theta_p$ of this vector. So we may say that the vector $\mathbf{J}$ starts at the crack tip and points into the direction of crack propagation. The angle of crack propagation is then derived from

$$\tan \theta_p = \frac{J_2}{J_1}. \tag{9}$$

The concept of the J-integrals has been developed further by Freund (1990) and Nishioka and Atluri (1983) for situations of dynamic fracture. Freund (1990) has proved that the energy release rate $\mathscr{G}(c)$ for a crack propagating at speed c is equal to the energy release rate $\mathscr{G}(0)$ for a stationary crack of the same length and subject to the same, instantaneous loading conditions, multiplied by a universal function $g(c)$ of the crack speed. We take the length of the vector $\mathbf{J}$ as the energy release

rate $\mathcal{G}(0)$ of the corresponding equilibrium situation with the stationary crack and impose that the dynamic energy release rate $\mathcal{G}(c)$ equals the critical value $\mathcal{G}_C$. We further assume that the crack propagation is unstable. Thus, we obtain the following equation for the crack speed:

$$\mathcal{G}(c) = g(c)\sqrt{J_1^2 + J_2^2} = \mathcal{G}_C, \tag{10}$$

where the function $g(c)$ of the crack speed is given by

$$g(c) = (1 - c/c_R)\sqrt{1 - c/c_d} \tag{11}$$

with $0 \leqslant c < c_R < c_d$ and c_d and c_R being the dilatational wave speed and the Rayleigh wave speed, respectively. See also Freund (1990), van Vroonhoven (1996a), and van Vroonhoven and de Borst (1997). The crack increment is calculated according to

$$\mathbf{x}_{\text{tip,new}} = \mathbf{x}_{\text{tip,old}} + \mathbf{c} \cdot \Delta t, \tag{12}$$

where the length of the vector $\mathbf{c}$ equals the crack speed c and its direction is determined by the angle θ_p. The time step Δt is subject to some restrictions in order to assure stability of the numerical time integration scheme; these restrictions are discussed in Section 4.

Alternatively, the direction of crack propagation can be decided on the basis of a simpler, "engineering" criterion: namely, in the direction perpendicular to the largest principal stress. To this end, the stress components σ_{ij} ($i, j = 1, 2$ or x, y) are calculated in all integration points of the three undamaged singular elements in the super element. Next, the stresses are calculated in the nodal points by a projection or extrapolation of the integration point stresses onto the nodes with a weighting of the contributions of the adjacent elements. These nodal point stresses are used to calculate an averaged principal stress in the following manner. We select the nodes in the super element, where the largest principal stress is positive and which are not part of the damaged element, and calculate the "average stress tensor" of the super element by averaging each stress component σ_{ij} over the selected nodes. The eigenvalues (the principal stresses) of the averaged stress tensor are denoted by σ_1 and σ_2 with $\sigma_1 \geqslant \sigma_2$. Finally, we define the largest principal stress of the super element as the largest eigenvalue σ_1 of the averaged stress tensor and take the direction perpendicular to this largest principal stress as the direction of crack propagation. This criterion is consistent with observations in compression tests on concrete specimens, where cracks grow parallel to the direction of the largest compressive principal stress σ_2 with $\sigma_2 < 0$. The crack speed c is set equal to the Rayleigh wave speed c_R and the relation (12) is used to determine the crack increment. The rough estimate of the Rayleigh wave speed is acceptable, because we mostly observe large value for the energy release rate in cases of dynamic fracture. Thus, the precise crack speed will not differ much from c_R as can be seen from (10) and (11). When the largest principal stress is negative, we put $c = 0$ and crack arrest occurs. The accuracy of this procedure is increased when the stresses are also evaluated in the undamaged variable-node elements of the super element. We shall use this refined procedure and compare the results with those of the J-integral criterion. Although the principal stress criterion has no profound basis in fracture mechanics, it appears to work rather well with reasonably accurate results for the crack patterns. We note that it can be worthwhile to investigate the possibilities of applying a similar engineering criterion based on principal strain directions, especially for the previously mentioned compression tests.

3.3. *Extension to three dimensions*

The combined fracture/damage approach can be extended to problems of crack propagation in three dimensions, with a restriction to thin plate-like structures having slight curvature and/or slight thickness variations. The division into finite elements is chosen to have only one element over the thickness of the plate. The curvature of the surfaces and the variations in the thickness are thus incorporated, while the computing time for the assembly process is limited. Using more elements over the thickness would increase the assembly time proportionally. Moreover, tensile forces and bending moments will be dominant in the loading of the plate. Since the corresponding internal stresses are constant or vary approximately linearly over the thickness of plate, a further refinement of the element division in the thickness direction is not considered necessary. A consequence of this choice of one element over the thickness is that the crack front must be taken as a straight line perpendicular to the middle plane of the plate. In practical fracture problems, however, the crack front may attain a general curved shape in a perpendicular cross section of the plate, due to different crack speeds in the upper and lower planes of the plate. These effects are not incorporated and can only be calculated by time-consuming computations with more than one element over the thickness. Concerning the geometry of the plate-like structure, we may certainly speak of a three-dimensional analysis, but regarding the fracture behaviour we employ the simplification of a crack which is uniform over the thickness with a straight crack front. This simplified crack representation is sufficiently detailed in the plane of the plate and is capable of correctly analyzing general crack propagation problems.

The extension of the two-dimensional super element to three dimensions is straightforward. We choose the eight-node brick elements of Wilson et al. (1973) and Taylor et al. (1976) with improved bending behaviour to divide the geometry into subdomains. The element division in the crack-tip region is adapted in such a manner that the upper and lower planes of the plate have geometries similar to the element division in Fig. 3, with the addition of 17 nodes in the upper plane and 17 nodes in the lower plane of the plate. Five mid-side nodes are added in the middle plane of the plate, on the lines connecting the corner nodes in the lower and upper planes of the singular elements, including an extra node on the crack front. Thus, the crack-tip elements resemble the element of Fig. 1(b) and the surrounding elements are the variable-node elements of Hughes (1987). The crack is represented by damaged elements having orthotropic constitutive behaviour with their stiffness reduced in the direction perpendicular to the crack surfaces.

The crack propagation criterion in three dimensions requires only little adaptation. The integrals J_k ($k = 1, 2$) are evaluated by integration over a cylinder surrounding the crack tip. The cross sections of the cylinder in the upper and lower planes of the plate coincide with the contour depicted in Fig. 5. Because of the integration over the plate thickness, the influences of both tension and bending are incorporated in the J-integrals and thus also in the crack propagation criterion. We define the vector $\mathbf{J} = J_k \mathbf{e}_k$ (with summation over $k = 1, 2$), where the unit vectors $\mathbf{e}_1$ and $\mathbf{e}_2$ are tangential and perpendicular to the crack and $\mathbf{e}_3 = \mathbf{e}_1 \times \mathbf{e}_2$ is perpendicular to the plate. The vector $\mathbf{J}$ is thus, in the tangent plane of the plate; if this vector has a non-zero component normal to the plate due to numerical round-off errors, we use its projection onto the tangent plane. The crack speed is now determined by equations (10) and (11) and the direction of crack propagation by (9).

The criterion based on the largest principal stress is also extended to three dimensions. The stress components σ_{ij} ($i, j = 1, 2, 3$ or x, y, z) are calculated in the integration points of the

undamaged elements of the super element, analogous to the criterion in two dimensions. This procedure automatically includes thickness effects and the influence of possible bending moments. The integration point stresses are projected or extrapolated to the nodal points and subsequently averaged per component. The eigenvalues of the averaged stress tensor are denoted by σ_i ($i = 1, 2, 3$) with $\sigma_1 \geqslant \sigma_2 \geqslant \sigma_3$. The direction of crack propagation is again determined as perpendicular to the direction of the largest eigenvalue σ_1 (the largest principal stress) of the averaged stress tensor. The crack propagation must also take place in the direction perpendicular to the vector $\mathbf{e}_3$ normal to the plane of the plate, i.e., take place in the tangent plane of the plate.

4. Time-step algorithm

4.1. *Explicit method*

The discretization of the elastic body into subdomains (finite elements) and the assembly of all element contributions into global matrices and vectors leads to the following matrix-vector equation

$$M \cdot \ddot{\mathbf{U}} + K \cdot \mathbf{U} = \mathbf{F}, \tag{13}$$

where M is the mass matrix, K is the stiffness matrix, and $\mathbf{F}$ is the right-hand side vector of the prescribed forces. The vector $\mathbf{U} = \mathbf{U}(t)$ is the global vector of nodal displacements. For the numerical solution of this second-order differential equation, we discretize the time interval in finite steps of size Δt and calculate the approximate solution on times $t_n = n\,\Delta t$ (for $n = 0, 1, 2, \ldots$). We choose an explicit method based on central differences. The first-order and second-order derivatives $\dot{\mathbf{U}}$ and $\ddot{\mathbf{U}}$ of the global displacement vector are then approximated by

$$\dot{\mathbf{U}}(t_{n+(1/2)}) = \frac{\mathbf{U}(t_{n+1}) - \mathbf{U}(t_n)}{\Delta t}, \tag{14}$$

$$\ddot{\mathbf{U}}(t_n) = \frac{\dot{\mathbf{U}}(t_{n+(1/2)}) - \dot{\mathbf{U}}(t_{n-(1/2)})}{\Delta t} = \frac{\mathbf{U}(t_{n+1}) - 2\mathbf{U}(t_n) + \mathbf{U}(t_{n-1})}{(\Delta t)^2}. \tag{15}$$

The truncation errors in these approximations are of the order $O((\Delta t)^2)$ for time steps $\Delta t \to 0$, so that the central difference method is second-order accurate. Substitution of (14) and (15) into (13) produces the following time-step algorithm. Firstly, the acceleration vector is calculated:

$$M \cdot \ddot{\mathbf{U}}(t_n) = \mathbf{F}(t_n) - K \cdot \mathbf{U}(t_n). \tag{16}$$

Secondly, the velocity and displacement vectors are updated:

$$\dot{\mathbf{U}}(t_{n+(1/2)}) = \dot{\mathbf{U}}(t_{n-(1/2)}) + \Delta t \ddot{\mathbf{U}}(t_n), \tag{17}$$

$$\mathbf{U}(t_{n+1}) = \mathbf{U}(t_n) + \Delta t \dot{\mathbf{U}}(t_{n+(1/2)}). \tag{18}$$

The initial values of the displacements and the velocities are assumed to be known: $\mathbf{U}(t_0) = \mathbf{U}_0$ and $\dot{\mathbf{U}}(t_{0-(1/2)}) = \dot{\mathbf{U}}_0$.

Since the truncation errors in (14) and (15) vanish in the limit as $\Delta t \to 0$, the time-step algorithm (16)–(18) is consistent with the differential equation (13). Convergence of the solution is now

assured when the algorithm satisfies the stability condition, i.e., when small numerical errors are not amplified by taking one time step. The central difference method is conditionally stable, which means that the time step must be sufficiently small. We have the following restriction (Hughes, 1987):

$$\Delta t \leqslant \Delta t_{\max} = \frac{2}{\omega_h}, \tag{19}$$

where ω_h is the maximum natural frequency of vibration of the system represented by the equation (13). This frequency depends on the element size h and the dilatational wave speed c_d and is proportional to c_d/h. The proportionality constant is related to the element type. From the relation (19) with $\omega_h \sim c_d/h$, it is clear that the time step Δt is restricted by the smallest element in the entire element division.

We can make an estimate of the maximum allowed time step in the combined approach. Let us denote the maximum time step for a four-node quadrangular element of size $h_q \times h_q$ by Δt_q. This time step is calculated from an eigenvalue analysis of the element mass and stiffness matrices. The critical time step in the combined approach is determined by the smallest side of the singular crack-tip elements, which has a length $h_s = h_q/\sqrt{2}$. Hughes (1987) has derived estimates of the critical time step for several elements, e.g., $\Delta t_{\max 2} = h/c_d$ for the two-node linear rod element, and $\Delta t_{\max 3} = h/\sqrt{6}\, c_d$ for the three-node quadratic rod element. These estimates are extended to the two- and three-dimensional elements in the following manner. We regard the one-dimensional estimate $\Delta t_{\max 2}$ with $h = h_q$ as a relative measure for the quadrangular or brick elements and $\Delta t_{\max 3}$ with $h = h_s$ as a relative measure for the singular elements. Next, we assume that the maximum allowed time step in the combined fracture/damage approach is equal to the critical time step Δt_q of the quadrangular elements, multiplied by the ratio $\Delta t_{\max 3}/\Delta t_{\max 2}$. Thus, we obtain

$$\Delta t \leqslant \frac{\Delta t_{max3}}{\Delta t_{\max 2}} \Delta t_q = \frac{h_s \Delta t_q}{h_q \sqrt{6}} = \frac{\Delta t_q}{2\sqrt{3}} = 0.289\, \Delta t_q. \tag{20}$$

Since this is a rough estimate, we shall adopt $\Delta t = 0.25\, \Delta t_q$ to assure the stability of the time-step algorithm. We note that this time step is one fourth of the time step for elasto-dynamic stress calculations without fracture. As a result, the combined fracture/damage approach will require approximately four times as many time steps than an elastodynamic calculation.

The solution for the acceleration vector $\ddot{\mathbf{U}}(t_n)$ in (16) is immediately obtained when the mass matrix M is a diagonal matrix. Since this is generally not the case, we apply a so-called "lumping" technique. The original mass matrix is replaced with the lumped matrix $\tilde{M}$ which is defined by placing the row sums on the diagonal:

$$\tilde{M}_{ij} = \begin{cases} \Sigma_k M_{ik}, & \text{if } i = j, \\ 0, & \text{otherwise.} \end{cases} \tag{21}$$

The errors introduced by the lumping of the mass matrix tend to cancel the errors from the time discretization (Hughes, 1987). Since $\tilde{M}$ is a diagonal matrix, the solution of the eqn (16) does not require the inversion of a matrix. Thus, the combination of the central difference method and the lumping technique provides an accurate and efficient time-step algorithm. The disadvantage of

conditional stability is not regarded as a major drawback, because the time step should not be too large in view of the truncation errors involved in (14) and (15) and thus also in (17) and (18).

4.2. *Implicit method*

The number of time steps can be decreased by the use of an implicit method for the time-step algorithm, because such methods are mostly unconditionally stable and do not impose a restriction on the time step. We choose the implicit α-method of Hilber et al. (1977), which is also described by Hughes (1987). When the displacements, velocities, and the accelerations at time t_n are known, these quantities at time t_{n+1} are calculated from the equations

$$M\cdot\ddot{\mathbf{U}}(t_{n+1})+(1+\alpha)K\cdot\mathbf{U}(t_{n+1})-\alpha K\cdot\mathbf{U}(t_n)=\mathbf{F}(t_{n+1}+\alpha\,\Delta t), \tag{22}$$

$$\mathbf{U}(t_{n+1})=\mathbf{U}(t_n)+\Delta t\dot{\mathbf{U}}(t_n)+\tfrac{1}{2}(\Delta t)^2[(1-2\beta)\ddot{\mathbf{U}}(t_n)+2\beta\ddot{\mathbf{U}}(t_{n+1})], \tag{23}$$

$$\dot{\mathbf{U}}(t_{n+1})=\dot{\mathbf{U}}(t_n)+\Delta t[(1-\gamma)\ddot{\mathbf{U}}(t_n)+\gamma\ddot{\mathbf{U}}(t_{n+1})]. \tag{24}$$

The α-method is unconditionally stable and second-order accurate when $\alpha\in[-1/3, 0]$, $\beta=(1-\alpha)^2/4$ and $\gamma=(1-2\alpha)/2$. It is assumed that the initial values of the displacements and the velocities, $\mathbf{U}(t_0)=\mathbf{U}_0$ and $\dot{\mathbf{U}}(t_0)=\dot{\mathbf{U}}_0$, are known. The initial acceleration $\ddot{\mathbf{U}}(t_0)$ may be determined from (22) with $\alpha=0$ and $n=-1$. The advantage of unconditional stability is that there is no restriction on the time step. So, we may choose larger time steps than in the explicit method, which makes the implicit method more suitable for the analysis of complex geometries with small elements.

The disadvantage of implicit methods is that a system of equations needs to be solved at every time step. The acceleration vector $\ddot{\mathbf{U}}(t_{n+1})$ is calculated, for example, by substitution of (23) into (22) and by solution of the matrix–vector equation with the use of direct or iterative techniques (Golub and Van Loan, 1983). This procedure requires extra computing time and diminishes the gain of fewer time steps. Moreover, the mass matrix M and the stiffness matrix K depend on the time step because of the crack propagation and of the moving super element. Consequently, the system of equations to be solved is different at every time step. For these reasons, the implicit α-method can be less suitable than the explicit method for systems with a large number of degrees of freedom and with crack propagation. The choice for an implicit method or an explicit method is, therefore, dependent on the problem that is to be analyzed.

5. Applications

The combined fracture/damage approach has been implemented in the programming environment MATLAB (1992). The generation of the finite element division has been done with the use of the program SEPMESH of the package SEPRAN (1993). Several tests have been performed to investigate the accuracy and reliability of this approach and to compare the results obtained with the two crack propagation criteria based on the J-integrals and on the largest principal stress. The results of these tests are discussed below.

5.1. *Square plate*

The first test concerns the possible dependence of the calculated crack patterns on the finite element division. We study a square plate of size $l \times l$ and thickness $h = l/4$, which is loaded by uniform tensile forces or uniform bending moments on two opposite sides. Thinner plates are not considered, because otherwise the critical time step becomes too small and impractical. The plate is divided into 10×10 or 16×16 elements with one element over the thickness. The slanted orientation of the element lines is at most 0.10 or 0.20, which corresponds to inclination angles of 5.7° and 11.3°, respectively.

A crack is initiated at the middle of one of the traction-free sides, with an initial length $\frac{5}{4} l_e$ with l_e the element width. We employ the explicit central-difference method as time-step algorithm and we assign a small value to the fracture toughness to enforce crack propagation. As a result, the crack speed is approximately equal to the Rayleigh wave speed c_R and the crack increment to $\Delta x = c_R \Delta t \approx l_e/10$. The computation terminates, when the crack path reaches the element on the opposite traction-free side at the boundary of the plate and the construction of a super element is not possible anymore. The calculated crack patterns in the plate loaded by tensile forces are shown in Fig. 6 for the principal stress criterion and in Fig. 7 for the *J*-integral criterion. The results are shown in the original element divisions for clarity. The crack patterns in the plate loaded by bending moments are similar to these results. The crack propagation should occur along straight lines, because the uniform tensile forces lead to a symmetric situation in which only the crack-opening mode (mode I) exists. Similarly, the uniform bending moments lead to a situation with only the normal-bending mode (mode 1). For the definition of the tensile and bending fracture modes we refer to Cherepanov (1979) and van Vroonhoven (1996a).

Regarding the crack patterns in Figs 6 and 7, we observe that the end points of the crack paths are always within one element from the prospective end points (marked by $\times$), which is considered as sufficiently accurate. We also observe that the results for the *J*-integral criterion are more sensitive to the skewed orientation of the element division than those for the principal stress criterion. This can be explained by the following argument. The contour for the computation of the *J*-integrals consists of seven segments (see Fig. 5), where five Gaussian integration points are used per segment in the circumferential direction and five in the thickness direction of the plate. This sums up to a total of 175 points where the stresses are evaluated. The criterion based on the largest principal stress uses the average of the stress tensors evaluated in all Gaussian integration points of ten elements, which yields a total of $10 \times 27 = 270$ points. This higher number of points for stress evaluation may explain the better performance of the principal stress criterion. The accuracy of the *J*-integral can be improved by taking a contour at larger distance from the crack tip, but then the algorithm needs more computing time and becomes less efficient. Although the crack propagation criterion based on the (averaged) largest principal stress has no solid foundation in fracture mechanics, we conclude that this criterion produces the best results for the crack patterns.

5.2. *Single-edge notched beam*

The second test is a single-edge notched shear beam (Iosipescu, 1967), which is a suitable test for a study of curvilinear crack propagation under shear loads. We adopt the same specimen

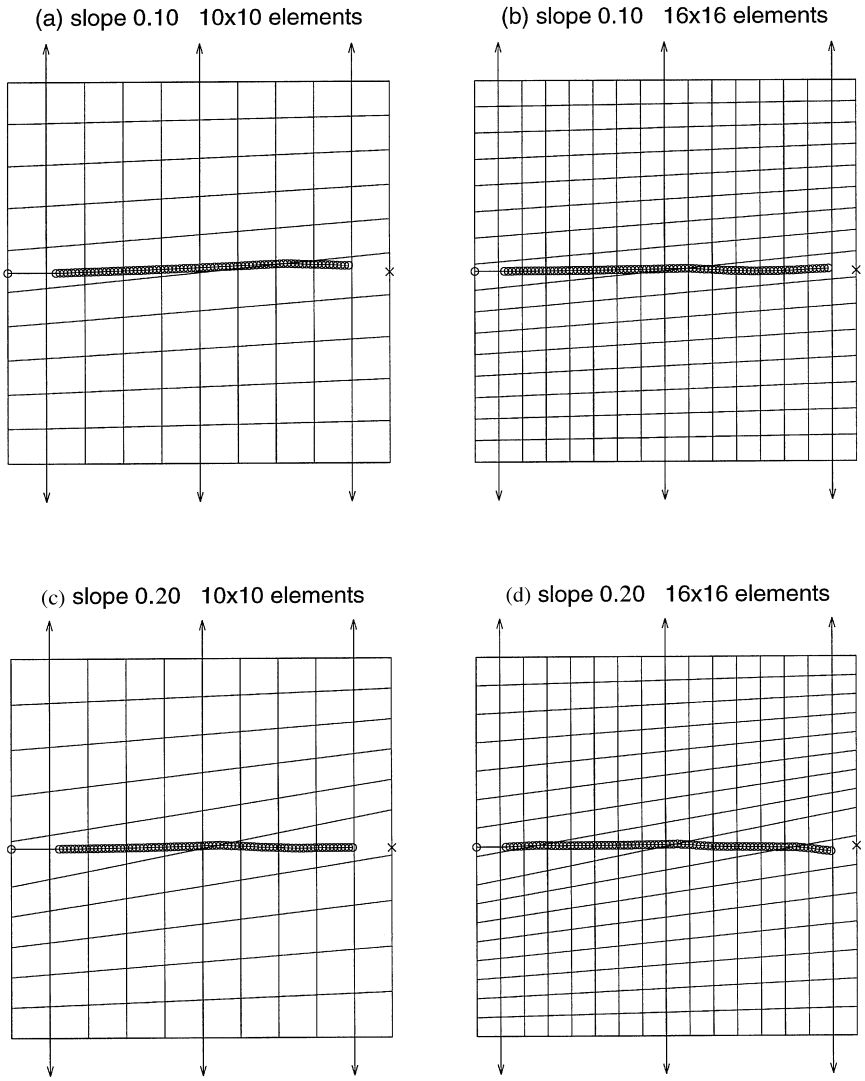

Fig. 6. Crack patterns in a square plate loaded by uniform tensile forces, for various element divisions. Subsequent positions of the crack tip are shown by ○ and the prospective end point of the crack by ×. Crack propagation criterion is based on largest principal stress.

dimensions as Feenstra (1993) and Schlangen (1993), viz. a length of 440 mm, a height of 100 mm, and a thickness of 10 mm. The forces F_1 are applied at a distance of 20 mm from the plane of symmetry and the forces $F_2 = F_1/10$ at a distance of 200 mm. The element division consists of 274 elements and is chosen such that the crack is not initiated at the boundary between two elements but in the interior of an element. The initial crack has a length of (a) 15 mm or (b) 25 mm and is located at the middle of the longest edge of the beam. The shear deformation leads to a situation

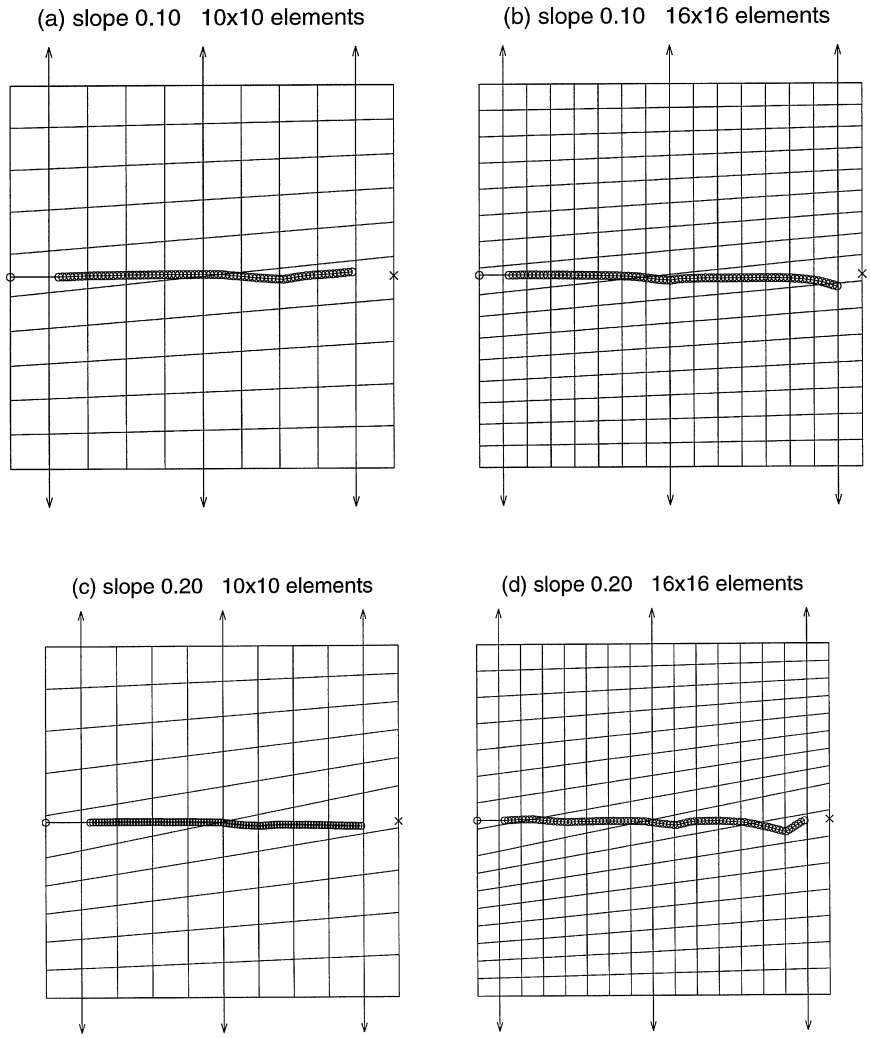

Fig. 7. Crack patterns in a square plate loaded by uniform tensile forces for various element divisions. Subsequent positions of the crack tip are shown by ○ and the prospective end point of the crack by ×. Crack propagation criterion is based on *J*-integrals.

where the crack-opening mode and the sliding mode are combined (modes I and II). We employ the implicit α-method with $\alpha = -0.3$ and use the crack propagation criterion based on the largest principal stress.

The obtained crack paths are shown in Fig. 8 and satisfy the requirement that the end points are on the opposite edge of the beam to the right of the point where the force F_1 is applied (Schlangen, 1993). Taking other time-step sizes leads to similar but not identical crack paths. Nevertheless, all crack paths lie within a small band around the paths shown in the figure and

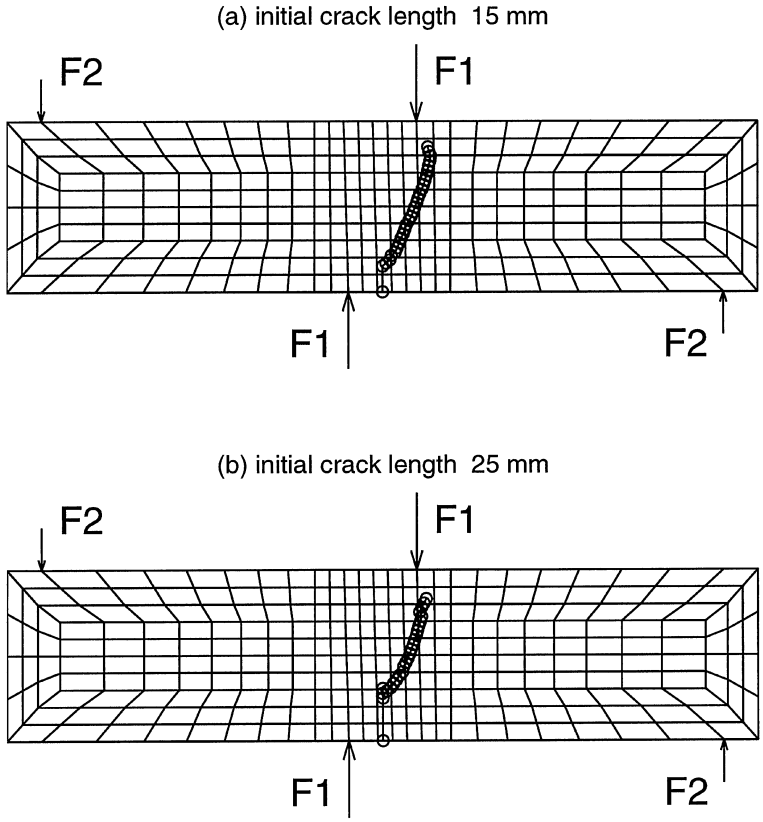

Fig. 8. Crack patterns in a single-edge notched beam loaded under shear conditions, for different initial crack lengths. Subsequent positions of the crack tip are shown by ○.

always satisfy the requirement for the end point. The calculated crack patterns agree with the results of Feenstra (1993) and Schlangen (1993) and also with those of Lubliner et al. (1989) and Rots (1991) who have applied a plastic fracture mechanism and a smeared crack representation, respectively. No acceptable results have been obtained with the use of the crack propagation criterion based on the *J*-integrals, which is due to the dominance of mode II in the early stage of fracture. This is a well-known problem of the *J*-integral criterion (Cherepanov, 1979).

5.3. *Hollow cylindrical pipe*

The third test concerns three-dimensional crack propagation in a hollow cylindrical pipe which is loaded by torsional moments at its ends. The pipe has a length 400 mm and inner and outer radii of 30 and 40 mm, respectively, such that the pipe thickness equals 10 mm. The division into finite elements contains 25 elements in the axial direction, 32 elements in the circumferential direction, and one element over the thickness. The division must have sufficient refinement for the construction of the super element. Otherwise, for coarser divisions, the added "slave" nodes of the

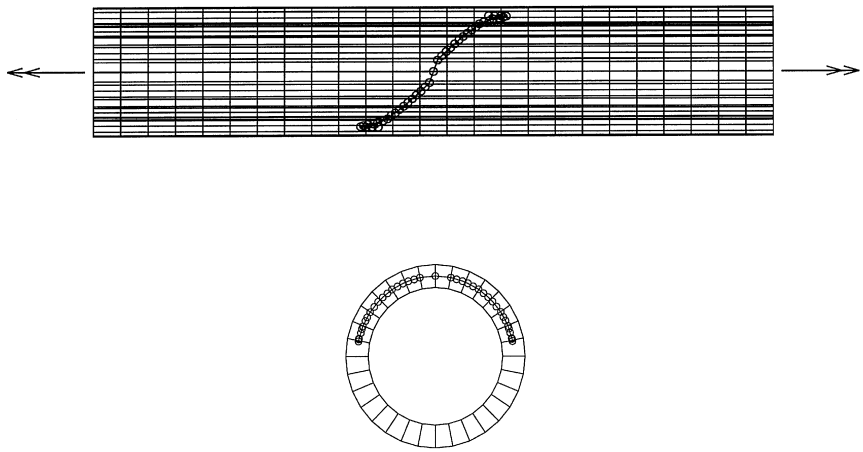

Fig. 9. Crack pattern in a pipe loaded by torsional moments. Initial crack is at middle of side view and at top of cross-sectional view. Subsequent positions of the crack tip (into two directions) are shown by ○.

super element can lie outside the domain occupied by the pipe due to the interpolation between the "master" nodes and due to the curvature of the elements and of the pipe surfaces.

A crack is initiated in the middle cross section of the pipe with initial length equal to 3/4 of the element size in the circumferential direction (approx. 4.58 mm). We use the explicit time-step algorithm in combination with the crack propagation criterion based on the largest principal stress, since the fracture process begins in mode II. Because of the restricted time step, the crack increments are approximately equal to 0.37 mm. We calculate the crack paths in two symmetric directions and terminate the calculation after 200 time steps. The results are shown in Fig. 9 for every tenth time step.

We observe some deviations in the crack pattern near the upper and lower boundaries in the side view of the pipe. These deviations are related to the plane drawing of the three-dimensional geometry and to the fact that the crack starts to propagate in the direction perpendicular to the axis of the pipe. At that moment, one half of the cross section has fractured and the pipe reaches the point of final collapse. Globally, the obtained crack paths are at an angle of 45° with the axial direction, which agrees with predictions based on the experimental results of Richard (1987) and on the analyses of Lakshminarayana and Murthy (1976).

6. Conclusions

The combined approach presented in this paper is based on the finite element method and combines the advantages of fracture mechanics and continuum damage mechanics. After the initialization of a crack and during the fracture simulation, a super element surrounding the crack tip is constructed and the crack path is modelled by softening elements. The singular crack-tip elements with quarter-point nodes provide sufficient accuracy for the calculation of the near-tip solution and the crack propagation. The representation of the crack by orthotropic softening elements provides sufficient flexibility to the approach and diminishes the necessary adaptations

of the finite element division. The rest of the structure is divided with the use of the so-called Wilson–Taylor elements, in order to prevent the system of equations from having excessive stiffness in situations with bending deformation. The crack propagation is decided on the basis of either the J-integrals or the largest principal stress in the crack-tip region. The former criterion has a profound basis in fracture mechanics and the latter one is based on a practical engineering rule.

The combined fracture/damage approach has been applied to a square plate loaded by tensile forces or bending moments, a single-edge notched beam subjected to shear, and a hollow cylindrical pipe subjected to torsion. Since damage mechanics methods are often sensitive to variations in the element division, possible element dependencies have been investigated. No serious dependencies on the element size or on the element orientation have been observed, although the results obtained with the principal stress criterion tend to be less sensitive to such variations than those obtained with the J-integral criterion. The results show that the calculated crack paths are always accurate within one element from the theoretical crack paths. This concerns both single-mode fracture (tension mode I or bending mode 1) and mixed-mode fracture (combination of tension mode I and shear mode II). The combined approach can also be applied to three-dimensional problems with dynamic loading and/or dynamic failure.

Acknowledgements

The authors wish to thank Dr J. Horsten (Philips Centre for Manufacturing Technology) for his contributions on numerical methods, and Prof. J. Boersma and Dr A. A. F. van de Ven (Eindhoven University of Technology, Faculty of Mathematics) for many helpful and stimulating discussions.

References

Barsoum, R. S. (1976) On the use of isoparametric finite elements in linear fracture mechanics. *International Journal of Numerical Methods in Engineering* **10,** 25–37.

Bažant, Z. P. and Cedolin, L. (1991) *Stability of Structures. Elastic, Inelastic, Fracture, and Damage Theories*. Oxford University Press, New York.

de Borst, R. (1993) A generalisation of J_2 flow theory for polar continua. *Computer Methods in Applied Mechanics and Engineering* **103,** 347–362.

de Borst, R., Sluys, L. J., Mühlhaus, H.-B. and Pamin, J. (1993) Fundamental issues in finite element analysis of localization of deformation. *Engineering Computations*. **10,** 99–121.

Broek, D. (1986) *Elementary Engineering Fracture Mechanics*. Kluwer Academic Publishers, Dordrecht, The Netherlands.

Chaboche, J. L. (1981) Continuum damage mechanics—a tool to describe phenomena before crack initiation. *Nuclear Engineering and Design* **64,** 233–247.

Chaboche, J. L. (1988a) Continuum damage mechanics: part I—general concepts. *ASME Journal of Applied Mechanics* **55,** 59–64.

Chaboche, J. L. (1988b) Continuum damage mechanics: part II—damage growth, crack initiation, and crack growth. *ASME Journal of Applied Mechanics* **55,** 65–72.

Cherepanov, G. P. (1979) *Mechanics of Brittle Fracture*. McGraw-Hill, New York.

England, A. H. (1965) A crack between dissimilar media. *ASME Journal of Applied Mechanics* **32,** 400–402.

Feenstra, P. H. (1993) *Computational Aspects of Biaxial Stress in Plain and Reinforced Concrete*. Ph.D. thesis, Delft University of Technology, The Netherlands.

Freund, L. B. (1990) *Dynamic Fracture Mechanics*. Cambridge University Press, Cambridge.

Golub, G. H. and Van Loan, C. F. (1983) *Matrix Computations*. North Oxford Academic, Oxford.

Hilber, H. M., Hughes, T. J. R. and Taylor, R. L. (1977) Improved numerical dissipation for time integration algorithms in structural dynamics. *Earthquake Engineering and Structural Dynamics* **5,** 283–292.

Horsten, J. and van Vroonhoven, J. (1994) A hybrid fracture-damage propagation model. *Localized Damage III, Computer-Aided Assessment and Control*. Proceedings of the 3rd International Conference on Localized Damage, Udine, Italy, pp. 367–374.

Hughes, T. J. R. (1987) *The Finite Element Method. Linear Static and Dynamic Finite Element Analysis*. Prentice-Hall, Englewood Cliffs, NJ.

Iosipescu, I. (1967) New accurate procedure for single shear testing of metals. *Journal of Materials* **2,** 537–566.

Kachanov, L. M. (1958) The time to fracture under creep conditions (translation from Russian). *Izvestiá Akademia Nauk SSSR, Otdel. Tekhn. Nauk* **8,** 26–31.

Lakshminarayana, H. V. and Murthy, M. V. V. (1976) On stresses around an arbitrarily oriented crack in a cylindrical shell. *International Journal of Fracture* **12,** 547–566.

Lasry, D. and Belytschko, T. (1988) Localization limiters in transient problems. *International Journal of Solids and Structures* **24,** 581–597.

Lemaitre, J. (1984) How to use damage mechanics. *Nuclear Engineering and Design* **80,** 233–245.

Lubliner, J., Oliver, J., Oller, S. and Oñate, E. (1989) A plastic-damage model for concrete. *International Journal of Solids and Structures* **25,** 299–326.

MacNeal, R. H. (1994) *Finite Elements: Their Design and Performance*. Marcel Dekker, New York.

MATLAB. (1992) *High-Performance Numeric Computation and Visualization Software. Reference Guide*. The MathWorks, Natick, MA.

Mühlhaus, H.-B. (1989) Application of Cosserat theory in numerical solutions of limit load problems. *Ingenieur Archiv* **59,** 124–137.

Murakami, S. (1988) Mechanical modelling of material damage. *ASME Journal of Applied Mechanics* **55,** 280–286.

Needleman, A. (1988) Material rate dependence and mesh sensitivity in localization problems. *Computer Methods in Applied Mechanics and Engineering* **67**, 69–85.

Nishioka, T. and Atluri, S. N. (1983) Path-independent integrals, energy release rates, and general solutions of near-tip fields in mixed-mode dynamic fracture mechanics. *Engineering Fracture Mechanics* **18,** 1–22.

Nishioka, T., Murakami, R. and Takemoto, Y. (1990) The use of the dynamic J integral (J') in finite-element simulation of Mode I and mixed-mode dynamic crack propagation. *International Journal of Pressure Vessels and Piping* **44,** 329–352.

Rice, J. R. (1968) A path independent integral and the approximate analysis of strain concentration by notches and cracks. *ASME Journal of Applied Mechanics* **35,** 379–386.

Richard, H. A. (1987) Safety estimation for construction units with cracks under complex loading. *Structural Failure, Product Reliability and Technical Insurance*, ed. H. P. Rossmanith, pp. 423–437. Interscience Enterprises, Geneva.

Rots, J. (1991) Smeared and discrete representations of localized fracture. *International Journal of Fracture* **51,** 45–59.

Schlangen, E. (1993) Experimental and numerical analysis of fracture processes in concrete. Ph.D. thesis, Delft University of Technology, The Netherlands.

SEPRAN. (1993) *Sepra Analysis. Users Guide and Programmers Manual*. Ingenieursbureau Sepra, Leidschendam, The Netherlands.

Sluys, L. J. (1992) Wave propagation, localisation and dispersion in softening solids. Ph.D. thesis, Delft University of Technology, The Netherlands.

Stern, M. (1979) Families of consistent conforming elements with singular derivative fields. *International Journal of Numerical Methods in Engineering* **14,** 409–421.

Stern, M. and Becker, E. B. (1978) A conforming crack tip element with quadratic variation in the singular fields. *International Journal of Numerical Methods in Engineering* **12,** 279–288.

Taylor, R. L., Beresford, P. J. and Wilson, E. L. (1976) a non-conforming element for stress analysis. *International Journal of Numerical Methods in Engineering* **10,** 1211–1219.

van Vroonhoven, J. C. W. (1996a) Dynamic crack propagation in brittle materials: analyses based on fracture and damage mechanics. Ph.D. thesis, Eindhoven University of Technology, The Netherlands.

van Vroonhoven, J. C. W. (1996b) Uncoupled dynamic fracture approach. *Mechanisms and Mechanics of Damage and Failure*. Proceedings of the 11th European Conference on Fracture ECF-11, Poitiers, France, pp. 455–460.

van Vroonhoven, J. C. W. and de Borst, R. (1997) Uncoupled numerical method for fracture analysis. *International Journal of Fracture* **84,** 175–190.

van Vroonhoven, J. C. W. and Horsten, J. B. A. M. (1966) Hybrid fracture/damage approach. *Mechanisms and Mechanics of Damage and Failure*. Proceedings of the 11th European Conference on Fracture ECF-11, Poitiers, France, pp. 975–980.

Wilson, E. L., Taylor, R. L., Doherty, W. P. and Ghaboussi, J. (1973) Incompatible displacement models. *Numerical and Computer Methods in Structural Mechanics*, eds. S. J. Fenves, N. Perrone, A. R. Robinson and W. C. Schnobrich, pp. 43–57. Academic Press, New York.